Effect of Cu substitution on the magnetic and magnetic induction heating response of $CdFe_2O_4$ spinel ferrite

R. Ghasemi[1,2], J. Echeverría[1,2], J.I. Pérez-Landazábal[1,2], J.J. Beato-Lopez[1,2], M. Naseri[3] and C. Gómez-Polo[1,2]

[1]Departamento de Ciencias, Universidad Pública de Navarra, Campus de Arrosadia, 31006 Pamplona, Spain.

[2]Institute for Advanced Materials (INAMAT), Universidad Pública de Navarra, Campus de Arrosadia, 31006, Pamplona, Spain.

[3]Department of Physics, Faculty of Science, Malayer University, Malayer, Iran.

Abstract.- In this work, a comparative study of the effect of Cu on the structural, magnetic and magnetic induction heating response in $CdFe_2O_4$ spinel is presented. The ceramic nanoparticles ($Cu_{1-x}Cd_xFe_2O_4$; $0 \leq x \leq 1$) were synthesized by co-precipitation from Cu(II), Cd(II) and Fe(III) salts. The samples, characterized by X-ray diffractometry, display the characteristic spinel cubic structure (space group *Fm3m*) where CdO is detected as main secondary phase (≈ 16% weight for $x = 1$). A high degree of nanoparticle agglomeration is inferred from the Transmission Electron Microscopy (TEM) images, as a consequence of the employed synthesis procedure. Regarding the magnetic properties, superparamagnetic behavior at room temperature can be disregarded according to the low field magnetization response (*ZFC-FC* curves). For $0.4 \leq x \leq 0.8$ ratios, the samples display maximum values in the magnetic moment that should be correlated to the cation distribution between the octahedral and tetrahedral sites. Maximum magnetization values lead to an enhancement in the magnetic induction heating response characterized by highest heating temperatures under the action of an *ac* magnetic field. In particular, maximum S*AR* values are estimated for $x = 0.8$ as a combined effect of high magnetic moment, low *dc* coercive field (high

susceptibility). Although these Cu-Cd ferrite nanoparticles display moderate *SAR* values (around 0.7 W/g), the control of the maximum heating temperatures through the cation distribution (composition) provides promising properties to be used as nanosized heating elements (i.e. hyperthermia agents).

Corresponding autor.-
Prof. Cristina Gómez-Polo
Departamento de Ciencias. Edificio de los Acebos.
Universidad Pública de Navarra. Campus de Arrosadia. 31006 Pamplona. Spain
Phone. +34-948169576; e.mail: gpolo@unavarra.es

Keywords.- magnetic nanoparticles; Cd ferrites; cation distribution; magnetic hyperthermia

1.- Introduction

Semiconductor ceramics represent an active current research topic in material science due to their applicability in different technological fields. In particular, a wide range of different applications has been proposed employing spinel ferrimagnetic ferrites (MFe_2O_4; *M*: Mn, Co, Ni. Cu): adsorbers and photocatalysts in the removal of contaminants in water [1, 2], gas sensors [3, 4], magnetic nanocarriers for biomedical applications as hyperthermia, drug delivery, MRI or MPI contrast agents [5, 6] and electromagnetic absorbers [7, 8]. In particular, Cu and Cd ferrites show excellent properties to be applied as efficient catalysts and chemical sensors [9-12], anode for lithium ion batteries [13, 14] or microwave electromagnetic absorbers [15, 16].

Spinel structure consists of a cubic compact package of oxygen anions in which cations occupy tetrahedral (*A*) and octahedral sites (*B*) [17]. The particular cation distribution depends on the composition and synthesis procedure and is usually characterized by the inversion parameter δ (fraction of divalent ions on the octahedral sites) [18]. Bulk $CdFe_2O_4$ is a normal spinel ($\delta = 0$) where Fe^{3+} cations occupy *B* sites and Cd^{2+} ions on *A* sites [19]. However, mixed spinel structures ($0 < \delta < 1$) are generally reported in nanostructured Cd ferrites, with Cd^{2+} cations distributed in both tetrahedral and octahedral sites [20]. The particular cation distribution plays a relevant role in physical parameters of these semiconductor ceramics. Particularly, the exchange coupling among ions in octahedral and tetrahedral sites (J_{BB} and J_{AA}) and the antiferromagnetic superexchange J_{AB} interaction between sites of different symmetry mainly control the magnetic properties in these ferrite spinel structures. Bulk normal ($\delta = 0$) $CdFe_2O_4$ displays antiferromagnetic behavior below

10 K as a consequence of the antiferromagnetic interaction between the Fe^{3+} cations (5 μ_B per Fe^{3+} ion) within the octahedral *B*-sites. However, room temperature ferrimagnetic response is reported in Cd ferrite nanoparticles due to the partial occupation of Fe^{3+} ions in the tetrahedral *A*-sites [21, 22]. In this case, the exchange antiferromagnetic *AB* interaction between both sublattices dominates. Furthermore, the occurrence of complex magnetic phenomena are also reported and related to non-collinear (canted) spin structures [23].

Regarding $CuFe_2O_4$ ferrite, partially inverted ($\delta \rightarrow 1$) spinel structure is usually reported with Cu^{2+} cations tending to occupy octahedral (*B*) sites and only a small amount of Cu^{2+} ions migrate from the octahedral (*B*) to tetrahedral (*A*) sites [24]. The ideal inverse configuration consists of Cu^{2+} on the octahedral sites and Fe^{3+} equally distributed between the tetrahedral and octahedral sites. Since the magnetization of *A* and *B* sublattices is antiparallel, being *A* and *B* sites ferromagnetically ordered, the total magnetic moment in this spinel comes from the uncompensated moments of the Cu cations (1 μ_B per ion). Therefore, the migration of Cu^{2+} ions from *B* to *A* sites (Fe^{3+} from *A* to *B*–sites) would give rise to a net increase in the magnetic moment of the spinel unit cell as a consequence of the unbalanced Fe^{3+} cation distribution. Due to the strong preference of Cd cations to the tetrahedral *A*- sites, the inclusion of Cd in the Cu ferrite leads to an increase in the magnetic moment (i.e. saturation magnetization) associated to the migration of the Fe^{3+} from *A* to *B*–sites. Moreover, Cd rich ferrites display reduced magnetization values as a consequence of the trend to the normal spinel configuration ($\delta = 0$) and the non-magnetic nature of the Cd^{2+} ions. Accordingly, maximum values of the saturation magnetization are experimentally observed in $Cu_{1-x}Cd_xFe_2O_4$ nanoparticles with $0 < x < 1$ [25-27]. In fact, similar magnetic response is

found in other mixed spinels (i.e. $Zn_{1-x}Co_xFe_2O_4$ [28-30]). In these ferromagnetic systems maximum saturation magnetization values are accompanied by a decrease in the effective Curie temperature as the Zn content increases as due to the weakening in *AB* superexchange interaction [31]. This behavior (increase in the effective magnetic moment accompanied by a decrease in the Curie point) enables the design of self-regulated magnetic hyperthermia systems [32]. Magnetic hyperthermia, associated to the temperature increase under the action of an *ac* magnetic field, has been widely analyzed in different magnetic nanoparticle systems [33]. Their main interest lies in the biomedical field, including different approaches as thermo ablation of tumors or drug delivery systems [34, 35]. While the increase in magnetization has generally associated an increase in the heating efficiency, the Curie point enables the control of the effective temperature of the hyperthermia therapy around therapeutic temperatures (45°C) [36]. However, these nanosized heating elements can be also employed in other technological fields: Magnetic Induction Swing Adsorption (MISA) systems (controlled gas capture and release) [37, 38]; new synthesis procedures of nanostructures [39, 40]; mechanical recovery or self-healing in polymers and glasses [41-45]; thermoplastic adhesives for bonded joints [46, 47]; heat assisted catalytic reactions [48, 49] and enhanced magnetic adsorbents in wastewater treatments [50].

Although previous studies reported the magnetic properties of Cu-Cd ferrite nanoparticles (i.e. occurrence of maximum values of saturation magnetization), a systematic analysis of the effect Cu substitution on characteristic magnetic parameters such as magnetic anisotropy is scarcely analyzed in the literature. Furthermore, the induction heating capacity (magnetic hyperthermia) of these ceramic nanosized systems has been barely reported.

Accordingly, in this work a comparative study of the effect of Cu on the structural, magnetic and magnetic induction heating response in $CdFe_2O_4$ spinel is performed. The ceramic nanoparticles ($Cu_{1-x}Cd_xFe_2O_4$; $0 \leq x \leq 1$), obtained by co-precipitation method, show the typical spinel structure. X-ray diffraction and Transmission Electron Microcopy (TEM) was employed to structurally characterize the samples. The magnetic response, characterized by SQUID magnetometry, indicates the occurrence of maximum magnetic moments for intermediate compositions $0.4 \leq x \leq 0.8$. Regarding the magnetic heating response, the results indicate a moderate heating response, where maximum heating efficiencies are mainly linked to the maximum magnetic moments for particular Cu-Cd intermediate compositions.

2.- Experimental procedure

Poly Vinyl Pyrrolidone (PVP), Iron nitrate $Fe(NO_3)_3.9H_2O$, Copper nitrate, $Cu(NO_3)_2 \cdot 3H_2O$, Cadmium nitrate, $Cd(NO_3)_2.4H_2O$, were used in the experiments, all with analytical grade. Deionized water was used throughout the experiments. $Cu_{1-x}Cd_xFe_2O_4$ (x = 0, 0.2, 0.4, 0.6, 0.8 and 1) nanoparticles were prepared in alkaline media from aqueous solutions [38]. Typically, 3.00 g of PVP were dissolved in 100 ml of deionized water at 353 K, and the obtained transparent solution was mixed with 0.20 mmol of iron nitrate and 0.10 mmol of a mixture of copper nitrate and cadmium nitrate (Fe:Cu, Cd = 2:1). After constant stirring for 2 h using a magnetic stirrer, the resultant homogeneous solution was added to a glass Petri dish where was heated at 363 K in an oven for 24 h in order to allow the evaporation of water. Afterwards, the obtained dried solid was ground for 20 min in a mortar to form powder. The powder was then annealed at 773 K for 9 h in order to obtain Cu-Cd ferrite nanoparticles.

X-ray measurements were carried out on a Siemens D-5000 powder diffractometer with monochromated Cu K_{α_1} radiation (λ= 1.54056 Å). Reflection X-ray powder diffraction data were collected from 20° to 70° in 2θ. The Rietveld Method and the Fullprof [51] program have been used to analyze the X-ray spectra. Transmission electron microscopy (HRTEM) and scanning transmission electron microscopy with a high angle annular dark field detector (STEM-HAADF) analysis were performed by using a FEI Tecnai Field Emission Gun operated at 300 kV. The magnetic response of the nanoparticles was analyzed through SQUID magnetometry (Quantum Design MPMS XL7). Finally, the magnetic induction heating (hyperthermia) curves under an *ac* field were measured with a home-made set up, composed of a *LC* resonant circuit connected to a 2 kW RF power amplifier (Electronic & Innovation, mod. 1240L). The time evolution of the temperature, *T*, of the nanoparticles in solid powder form (mass, m_{MNP} = 30 mg) was measured with a fibre optic thermometer (Neooptics, mod. T1) under an ac magnetic field (frequency 340 kHz and amplitude 384 Oe).

3.- Results and discussion

Firstly, the phase distribution was analysed through X-ray diffraction. The results indicate the coexistence in all the samples of the characteristic cubic spinel structure and a small fraction of CdO phase. As an example, Fig. 1 shows the X-ray diffraction pattern measured in the $CdFe_2O_4$ sample (black Points) and the Rietveld refinement (full line) using the crystallographic structures of the Cd-spinel and the CdO both with the same space group *Fm3m*. The difference between experimental and theoretical values are shown at the bottom of the figure. Hematite with a rhombohedral corundum structure (Space group *R3c*) cannot

be detected. Furthermore, for $CuFe_2O_4$ the low temperature tetragonal phase is not found, but the high temperature cubic phase characterizes the X-ray diffraction pattern. Actually, it is found that the formation of $CuFe_2O_4$ with tetragonal or cubic structure depends on different factors such as preparation method, synthesis conditions and annealing temperatures [52].

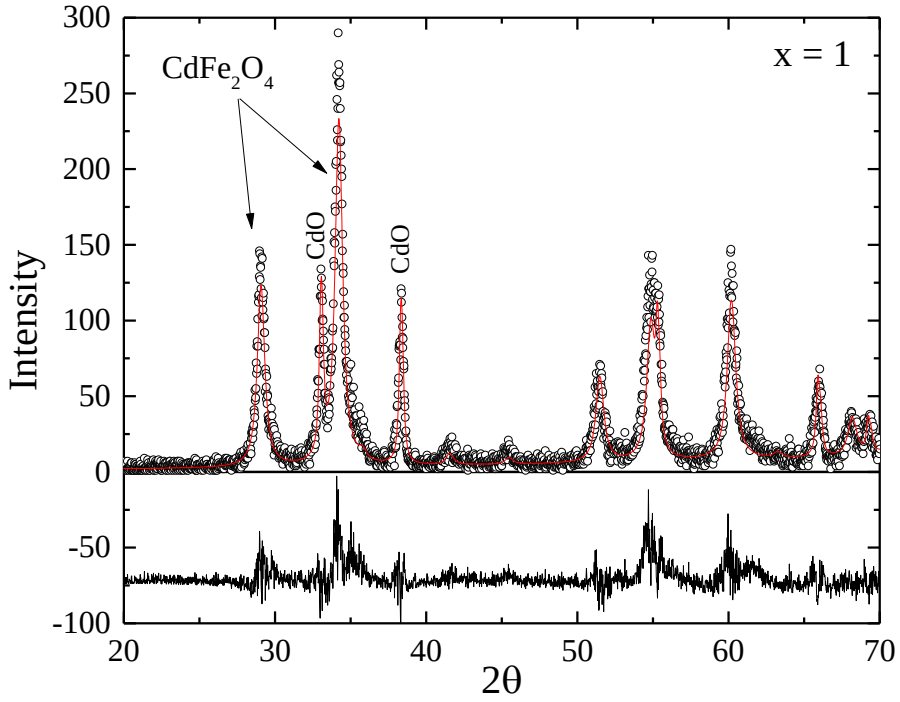

Fig 1. X-ray diffraction patter of $CdFe_2O_4$ nanoparticles

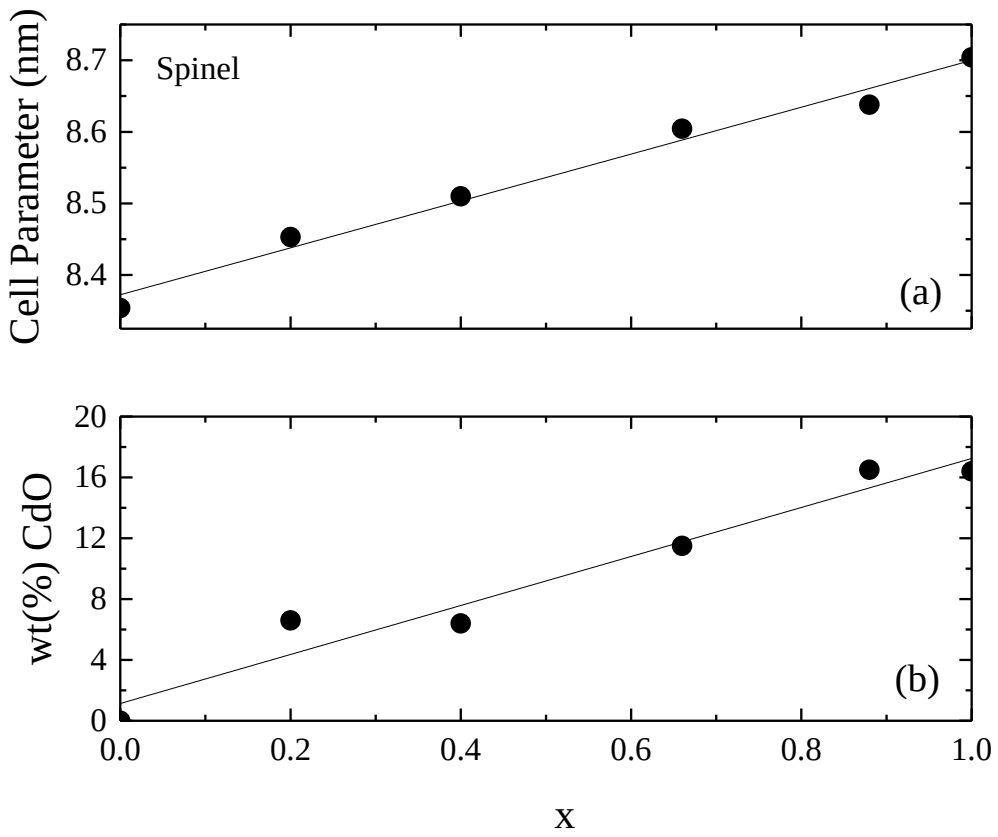

Fig 2. (a) Lattice cell parameter and (b) weight % of CdO phase as a function of Cd percentage *x* ($Cu_{1-x}Cd_xFe_2O_4$.).

The evolution of the cell parameter, *a*, as a function of Cd content (*x*) is shown in Fig. 2a. The changes of the cell parameter with *x* should be ascribed to the substitution of Cd^{2+} with larger ionic radius ($0.78A^{\circ}$) by Cu^{2+} ions ($0.57A^{\circ}$). Similar results have been previously reported in the literature [25-27]. Regarding the occurrence of the CdO secondary phase, an almost linear increase in the weight percentage with *x* is detected, (see Fig. 2b) reaching a maximum value around 16% for the $CdFe_2O_4$ sample.

Furthermore, TEM analysis shows a uniform particle size distribution with a high degree of agglomeration. Fig. 3 displays the obtained micrographs for *x* = 1, 0,8, 0.6 and 0.

The high degree of nanoparticle agglomeration is a direct consequence of the employed synthesis procedure [53]. In this case, it is not possible to detect a clear decrease in the mean nanoparticle size with the Cd content as reported in other studies [25, 26]. In fact, the average crystallite size, *d*, calculated by considering the strongest peak (311) and using Debye-Scherrer equation, leads to the following estimated values: 31 nm (x = 1), 13 nm (x = 0.8),18 nm (x = 0.6), 21 nm (x = 0.4), 18 nm (x = 0.2), 27 nm (x = 0).

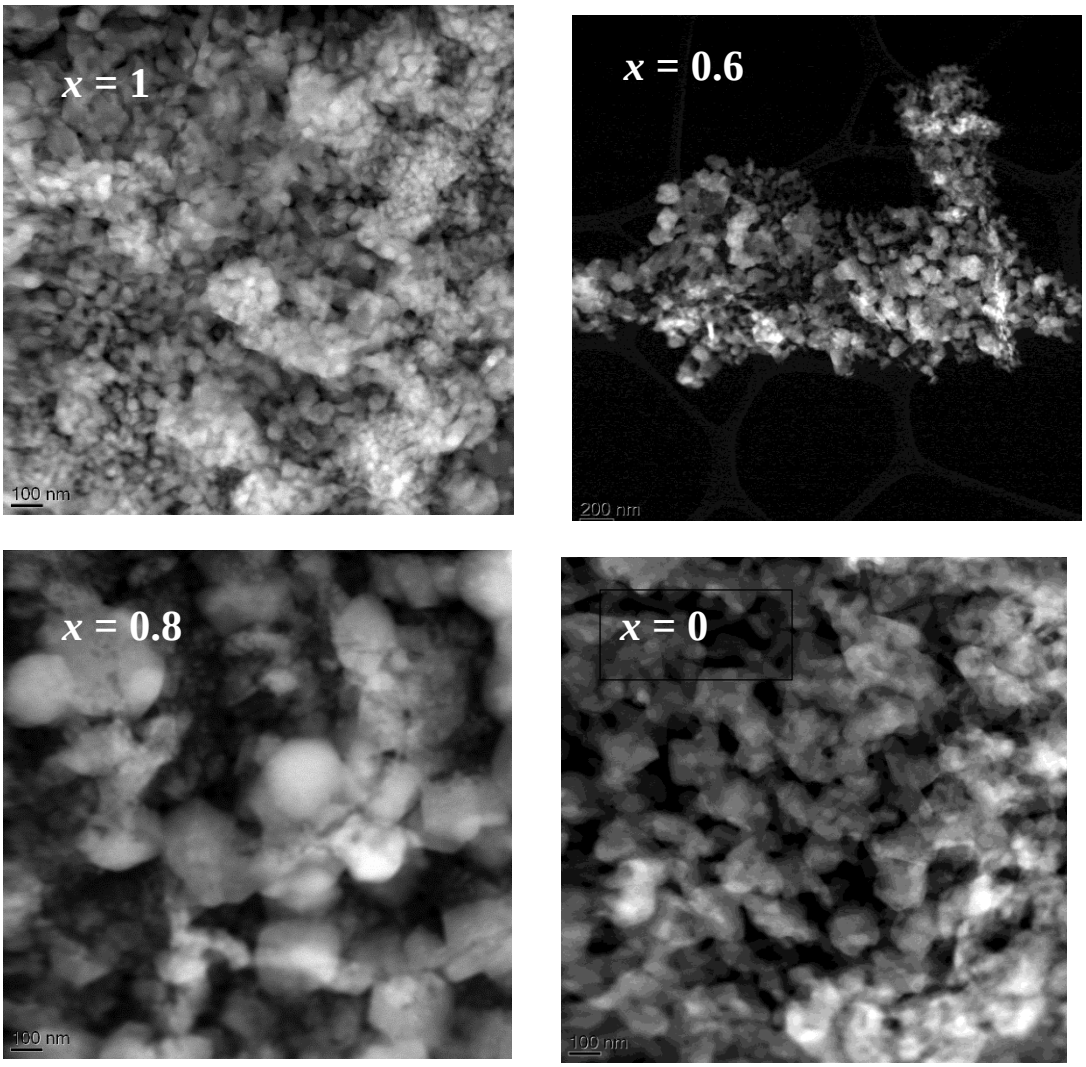

Fig 3. TEM images of $Cu_{1-x}Cd_xFe_2O_4$ nanoparticles.

With respect to the magnetic properties, Fig, 4 displays the temperature dependence of the high field magnetization, *M* (applied magnetic field $\mu_0 H$ = 6 T). A maximum value in *M* is found for *x* = 0.4. In order to evaluate the evolution of *M* with the temperature, *M(T)* was fitted at low temperature (*T* < 100 K) to the Bloch's law:

$$M(T) = M_S(0)[1 - BT^{\alpha}] \quad (1)$$

with $M_S(0)$ the magnetization at 0 K, *B* the Bloch constant and α a parameter which value depends on the size of the particles. Table I summarized the obtained results. Firstly, the Bloch constant decreases as the Cd is partially substituted by Cu, displaying similar values than those reported in other ferrite nanoparticles [54, 55]. Regarding α parameter, it ranges between the reported values in bulk systems (α = 3/2) and those obtained in the nanoscale (coming closer to 3 for small clusters) [56].

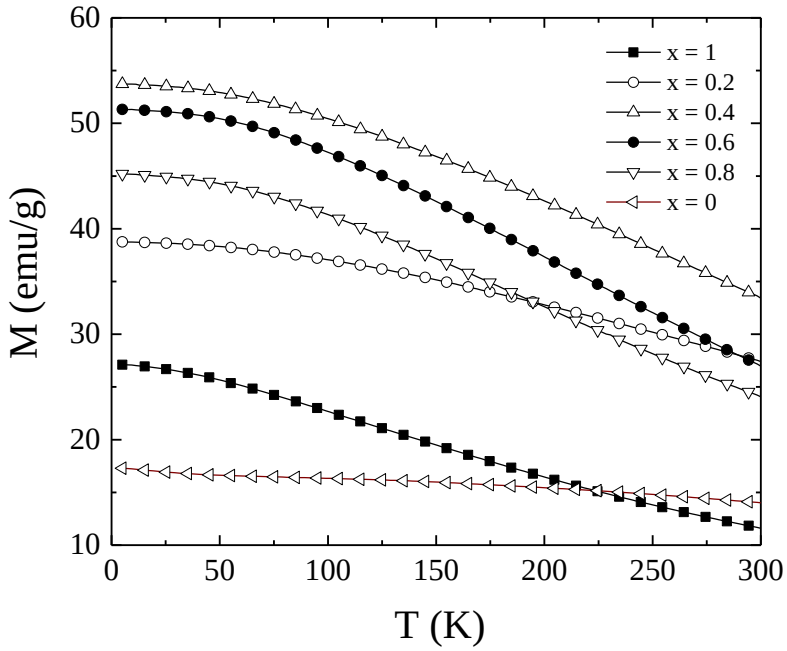

Fig. 4. High field magnetization curves (applied field $\mu_0 H$ = 6 T) for $Cu_{1-x}Cd_xFe_2O_4$ nanoparticles.

Table I: Magnetic parameters obtained from the fitting of *M(T)* to the Bloch's law (eq. 1) and the estimated magnetic moment, number of Bohr magnetons, n_B, per formula unit ($Cu_{1-x}Cd_xFe_2O_4$).

x	$M(0)$ (emu/g)	B (10^{-6} $K^{-\alpha}$)	α	n_B
1	27.21	138.0	1.54	1.7
0.8	45.25	13.3	1.90	2.6
0.6	51.36	6.0	2.05	2.7
0.4	53.8	13.5	1.83	2.7
0.2	38.77	7.8	1.87	1.8
0	16.6	0.6	2.2	0.7

With respect to the low field magnetization (i.e. *dc* magnetic susceptibility), Fig. 5 shows the *ZFC-FC* curves under an applied magnetic field of 50 Oe for the set of analyzed nanoparticles. The occurrence of superparamagnetic behavior at room temperature can be disregarded since a clear irreversible behavior between both magnetization curves is found for $T < 300$ K in all the samples. For $x > 0.4$ the samples display at low temperatures ($T < 50$ K) a decrease in both *ZFC-FC* magnetization curves. This behavior could indicate a certain degree of magnetic frustration at low temperatures (i.e. spin-glass state) as previously reported in other ferrite nanoparticle ferrites [30, 57]. The occurrence of Fe secondary phases in the $CuFe_2O_4$ cannot be excluded looking at the kink in both *ZFC-FC* magnetization curves around 150 K (i.e. Verwey transition of Fe_3O_4) [58].

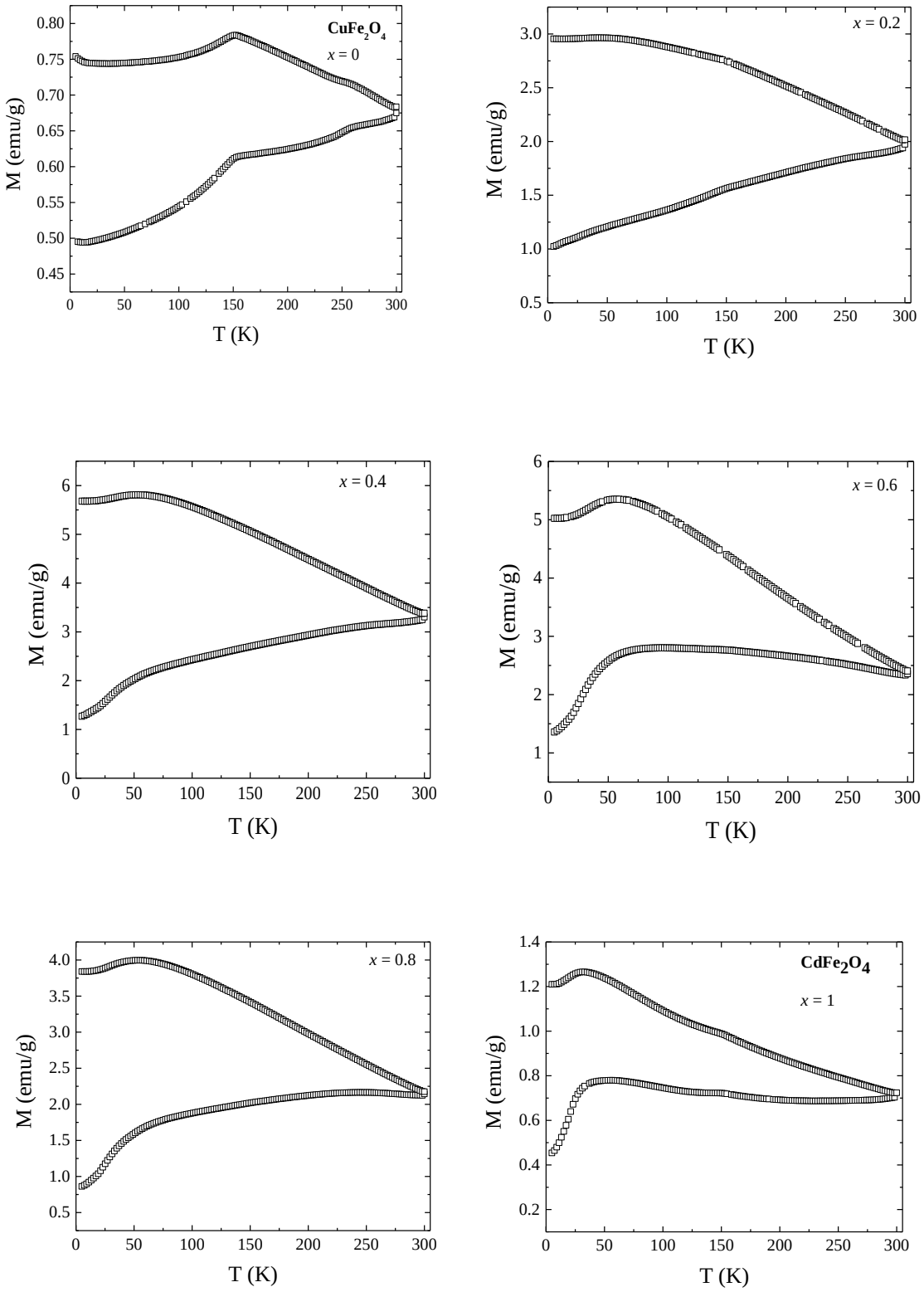

Fig. 5. *ZFC-FC* curves of $Cu_{1-x}Cd_xFe_2O_4$ nanoparticles (applied magnetic field H = 50 Oe).

As previously described, a maximum value in magnetization can be detected for x = 0.4. This result should be interpreted as a consequence of the cation (Cu, Cd) distribution between the spinel octahedral and tetrahedral sites. To confirm the contribution in the magnetization of the non-magnetic (diamagnetic) CdO, *M(0)* values where corrected taking into account the estimated *wt(%)* CdO from Fig. 2b (*M(0)* (corrected) = *M* (0)/(1- *wt(%)* CdO). As can be deduced from Fig. 6, such corrections do not introduce significant changes in *M* values. With respect to the magnetic moment, Table I summarizes the number of Bohr magnetons, n_B, per formula unit employing the corrected values of *M(0)* ($n_B = \frac{M_w M(0)(corrected)}{5585}$; M_w: molecular weight). Equivalently, maximum n_B values are found for $0.4 \leq x \leq 0.8$.

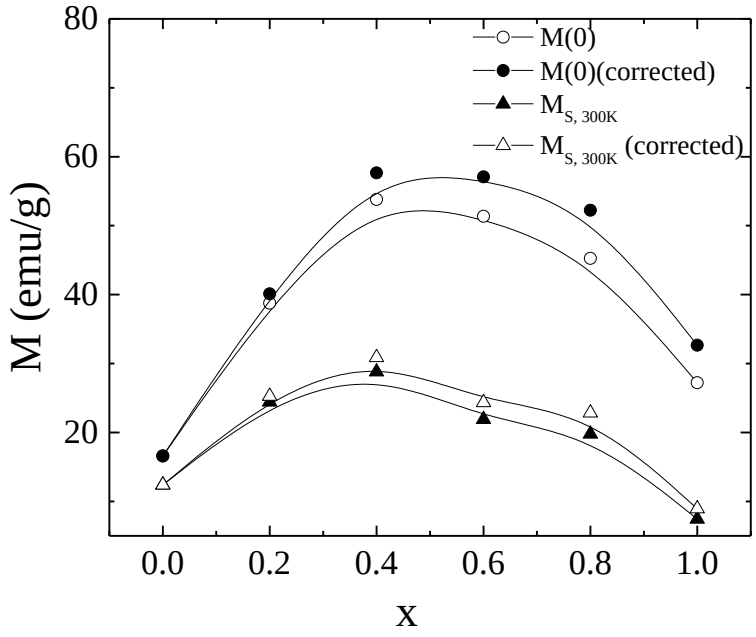

Fig 6. Saturation magnetization *M(0)* obtained from the Bloch's law (eq. 1) and from the law of approach to saturation M_S at 300 K (eq. 2) as a function of Cd percentage x ($Cu_{1-x}Cd_xFe_2O_4$.). the corrected values taking into account *wt(%)* CdO are also displayed.

With the aim to characterize the magnetic properties of the nanoparticles at room temperature, *dc* hysteresis loops were measured for the set of analysed samples (see Fig. 7). Maximum magnetic moments correspond with low values (close to the limit of the SQUID resolution) of coercive field, H_C (see Table II). However, as Fig. 7 shows, the samples do not reach the magnetic saturation at room temperature under the maximum applied field ($\mu_0 H$ = 6 T). Accordingly, the approach to saturation law was applied to fit the reversible magnetization response (*M*-*H*) curves in the range of applied fields from 3 to 6 T [59]:

$$M(T) = M_S(T)\left(1 - \frac{a}{H} - \frac{b}{H^2}\right) + \chi_{hf} H \qquad (2)$$

where M_S is the saturation magnetization and χ_{hf} the high field susceptibility resulting from the linear increase in magnetization by the application of *H*.

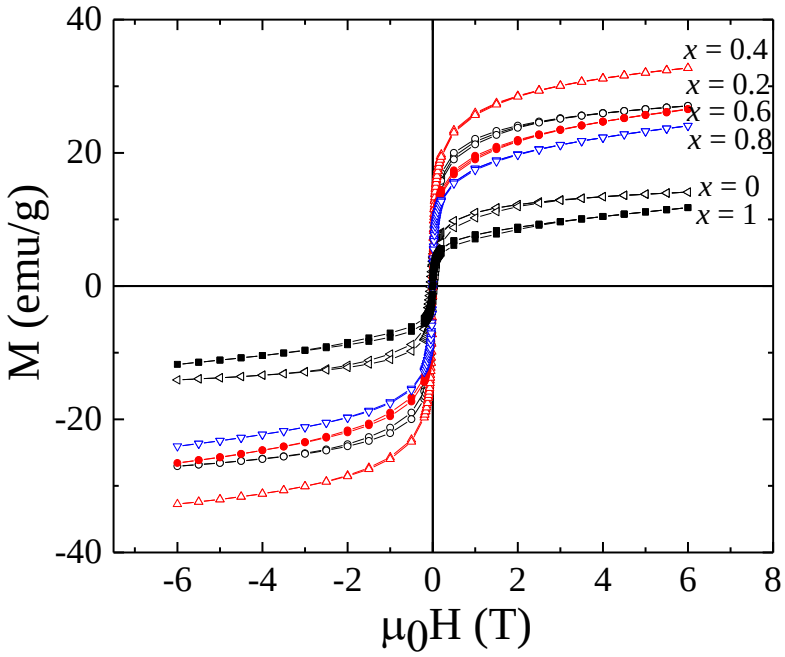

Fig. 7. *M*-*H* hysteresis loops at 300 K.

For the case of independent grains with cubic symmetry, the anisotropy term b/H^2 is

correlated to the magnetocrystalline anisotropy, K, by $b = \frac{8K^2}{105{M_S}^2}$. The term a/H, associated to the contribution of local inhomogeneities (i.e. structural defects, non-magnetic inclusions or microstresses), should be fixed equal to 0 to properly fit the experimental curves. The obtained fitted parameters as a function of the Cd content (x) of the nanoparticles are summarized in Table II. As expected from the previous analysis (Figs. 4 and 7), the saturation magnetization, M_S, displays a maximum value for Cd concentration x = 0.4. A proper correction taking into account the weight percentage of CdO does not significantly modify the trend of M_S vs x (see Fig. 6).

Table II: Magnetic parameters obtained from the room temperature hysteresis loops at 300 K and initial slope in the magnetic induction heating experiments.

x	H_C	M_S	b	K	χ_{hf}	$\left.\frac{dT(t)}{dt}\right\|_{t\to 0}$
	(Oe)	*(emu/g)*	*(10^7 Oe^2)*	*(10^5 erg/cm^3)*	*(10^{-5} Oe^{-1})*	*(Ks^{-1})*
1	90	7.44	2.37	1.6	3.0	0.10
0.8	10	19.79	3.80	5.1	4.7	0.91
0.6	36	21.90	3.58	5.3	7.0	0.24
0.4	24	28.81	2.41	5.5	8.2	0.31
0.2	92	24.42	2.43	4.5	7.4	0.38
0	481	12.4	2.55	2.7	6.4	0.05

Regarding the magnetic anisotropy, the estimated values are of the same order of magnitude of bulk magnetite ($K = 1.35\times10^5$ erg/cm^3). However, ferrite nanoparticles usually display higher effective anisotropy values attributed to surface spin disorder effects. In fact, higher anisotropy values (close to one order of magnitude higher, $K \approx 10^6$ erg/cm^3) are estimated in Co-Zn ferrites employing similar approach to saturation analysis [30]. The occurrence of the high field susceptibility term χ_{hf} also represents a common feature in

nanoparticle systems [60], and can be correlated to the occurrence of canted spin arrangement (Yafet-Kittel angle) in the spinel lattice [30].

Finally, the samples in powder form were submitted to the action of *ac* magnetic field, H_{ac}, to explore their characteristics for induction heating elements. Fig. 8 shows the time (t) evolution of the temperature, T, under the action of the alternating magnetic field. The temperature increases reaching a nearly constant value due to the non-adiabatic experimental conditions. Under these conditions, there is a heat balance between the heat generated by the magnetic nanoparticles and heat losses. Switching off H_{ac} magnetic field (see Fig. 8) gives rise to a sharp temperature decay associated to the quick heat dissipation due to the non-adiabatic conditions and the thermal interaction with the environment.

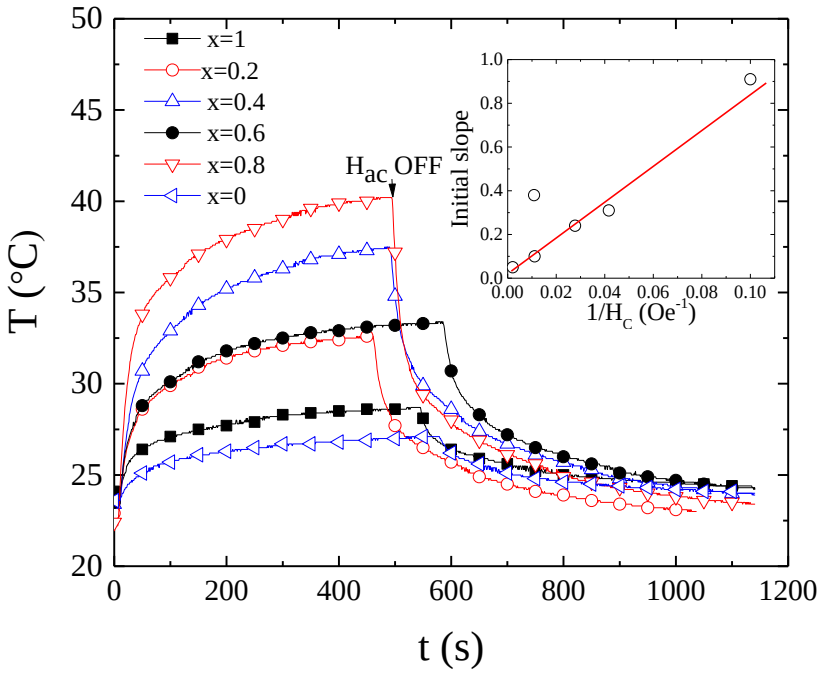

Fig. 8. Temperature, T, versus induction time, t, for the ($Cu_{1-x}Cd_xFe_2O_4$) nanoparticles. Inset: Initial slope $\left(\frac{dT(t)}{dt}\Big|_{t\to 0}\right)$ versus the inverse of the dc coercive field, H_C.

Under isoperibol conditions where the temperature of the sample varies but the temperature of its environment remains constant, the specific absorption rate, *SAR*, can be estimated through initial slope method [61]:

$$SAR = \frac{C}{m_{MNP}} \frac{dT(t)}{dt}\Big|_{t\to 0} \quad (3)$$

where C is the heat capacity of the system (measured in J K^{-1}), m_{MNP} the nanopartciles mass and $\frac{dT(t)}{dt}\Big|_{t\to 0}$ the initial T-t slope. Assuming a linear temperature dependence of the heat power losses, T vs t can be expressed for heating and cooling as $T(t) = T_0 + \Delta T_{max}\left(1 - e^{-t/\tau}\right)$ (Box-Lucas law) and $T(t) = T_0 + \Delta T_{max}\left(e^{-t/\tau}\right)$, respectively, with $\Delta T_{max} = T_{max} - T_0$ (T_{max}: maximum temperatures). In both cases, τ represents a time constant related to the thermal characteristics of the system [61] and thus $\frac{dT(t)}{dt}\Big|_{t\to 0} = \frac{\Delta T_{max}}{\tau}$. Table II includes the estimated initial slope obtained from the fitting of the exponential temperature increase to the Box-Lucas law. As deduced from the experimental curves, maximum T_{max} corresponds with a maximum value in the initial slope. Surprisingly, the sample with $x = 0.8$ displays maximum heating power capacity. A careful inspection of the room temperature coercive field (see table II) shows that this sample displays the smallest *dc* coercivity. In fact, as the inset of Fig. 8 indicates a linear relationship between the initial slope and the inverse of H_C ($H_C^{-1} \propto \chi$, magnetic susceptibility) can be deduced. Although the magnetic heating induction is determined by the *ac* hysteresis losses of the sample, the analysis of the quasistatic magnetic response gives some hints about the main parameters controlling the heating capacity of the samples: high magnetic moment (magnetization) and low *dc* coercive field. The low H_C values would favor the *ac* magnetization process under the *ac* magnetic field. However, the lowest coercivity is not reflected in the estimated high field anisotropy,

K, as no clear relationship between both magnitudes is found (see table II). Moreover, it should be noted that the heating behavior is a temperature dynamic effect and that, in turn, the increase in the temperature may modify the magnetic parameters. Particularly, the proximity of the Curie point, T_C, has associated a sharp increase in the magnetic susceptibility (Hopkinson effect) [62]. A large reduction of T_C with the Cd content (x) is found in these spinels [63] as a consequence of weakening of the *AB* interaction as the non-magnetic Cd^{2+} ions occupy the tetrahedral positions. In particular, values around $T_C \approx 400$ K are reported in bulk $Cu_{0.2}Cd_{0.8}Fe_2O_4$ (x = 8), close to the measuring temperature in the performed experiments. Thus, the proximity of the Curie temperature to room temperature for x = 0.8 would also contribute to the maximum values in T_{max} and in the initial heating slope. Nevertheless, these nanoparticles displays a moderate heating capacity in comparison with other nanoparticle systems employed for hyperthermia applications. In fact, assuming specific heat $c \approx 0.6$-0.8 $Jg^{-1}K^{-1}$, maximum SAR values around 0.7 W/g are achieved for x = 0.8, less than one order of magnitude than the typical *SAR* values reported in other Fe based ferrites. However, the possibility to optimize the magnetization values together with the reduction of the Curie point with the Cd content around therapeutic temperatures, provides to these spinel ferrites interesting properties to be applied as self-regulated heating agents, in the biomedical field (therapeutics agents and drug delivery systems) or environmental applications (catalysts and chemical and gases adsorbers) or self-healing of polymers and thermoplastic adhesives.

4. Conclusions

$Cu_{1-x}Cd_xFe_2O_4$ ($0 \leq x \leq 1$) nanoparticles were synthesized by co-precipitation from Cu(II), Cd(II) and Fe(III) salts. The structural characterization, performed by X-ray diffractometry and TEM microscopy, show that the nanoparticles display the characteristic cubic spinel structure with lattice parameter increasing with the Cd content. A high degree of nanoparticle agglomeration is found associated to the employed synthesis procedure. The magnetic characterization, both at low and high applied magnetic field, indicates the occurrence of maximum values in the magnetic moment for intermediate Cd concentrations ($0.4 \leq x \leq 0.8$). The samples display the characteristic features of nanoparticle ferrites (i.e. large temperature exponent in Bloch's law and high field susceptibility). Nevertheless, the occurrence of superparamagnetic behaviour should be disregarded as the *ZFC-FC* magnetization curves show. Regarding the magnetic heating induction response, maximum heating efficiency (i.e *SAR* value) is found for $x = 0.8$ that should ascribed to the combined effect of the high magnetic moment and high magnetic susceptibility (low coercive field). The control of the maximum heating temperature through the magnetic moment and the Curie temperature through the spinel composition (cation distribution), makes these ceramic nanoparticles interesting systems to be applied in a wide range of applications including, among others, hyperthermia treatments in the biomedical field and heat assisted catalytic and adsorption elements in environmental areas.

Acknowledgements

The work has been performed within the framework of projects MAT2017-83631-C3-2-R (Spanish "Ministerio de Economía, Industría y Competitividad") and DRUG-MAG,

Nueva generación de plataformas teragnósticas contra el cáncer asistidas por partículas superparamagnéticas (Gobierno de Navarra, Departamento de Desarrollo Económico). The microscopy works have been conducted in the "*Laboratorio de Microscopias Avanzadas*" at "*Instituto de Nanociencia de Aragon - Universidad de Zaragoza*". R. Ghasemi acknowledges the Iranian Ministry of Science, Research and Technology for the financial support at the Universidad Pública de Navarra.

References

1.- K. K. Kefeni, B. B. Mamba, T.A.M. Msagati, *Application of spinel ferrite nanoparticles in water and wastewater treatment: A review*, Sep. Purif. Technol. 188 (2017) 399-422.

2.- C.M. Parka, Y. M. Kim, K.-H. Kim, D. Wang, C. Sue, Y. Yoon *Potential utility of graphene-based nano spinel ferrites as adsorbent and photocatalyst for removing organic/inorganic contaminants from aqueous solutions: A mini review,* Chemosphere 221 (2019) 392-402

3.- K. Wu, J. Li, C.Zhang *Zinc ferrite based gas sensors: A review*, Ceram. Int. 45 (2019) 11143-11157.

4.- Y. Ma, Y. Lu, H. Gou, W. Zhang, S. Yan, X. Xu, *Octahedral $NiFe_2O_4$ for high-performance gas sensor with low working temperature,* Ceram. Int. 44 (2018) 2620-2625.

5.- M. Amiri, M. Salavati-Niasarib, A. Akbari, *Magnetic nanocarriers: Evolution of spinel ferrites for medical applications,* Adv. Colloid Interfac. 265 (2019) 29-44.

6.- N. Sanpo, C. C. Berndt, C. Wen, J. Wang, *New Approaches to the Study of Spinel Ferrite Nanoparticles for Biomedical Applications,* M. Aliofkhazraei, A.S.H. Makhlouf (eds.), Handbook of Nanoelectrochemistry, Springer International Publishing Switzerland 2016; *DOI 10.1007/978-3-319-15266-0_12*, 1417-1441.

7.- T. Sodaee, A. Ghasemi, R. S. Razavi, *Cation distribution and microwave absorptive behavior of gadolinium substituted cobalt ferrite ceramics,* J. Alloy. Compd. 706 (2017) 133-146.

8.- K. Chandra Babu Naidu, W. Madhuri, W. *Microwave processed bulk and nano NiMg ferrites: A comparative study on X-band electromagnetic interference shielding properties*, Mater. Chem. Phys. 187 (2017) 164-176.

9.- S.S. Selima, M. Khairy, M.A. Mousa, *Comparative studies on the impact of synthesis methods on structural, optical, magnetic and catalytic properties of $CuFe_2O_4$,* Ceramics. Int. 45 (2019) 6535-6540.

10.- S.B. Patil, H.S. Bhojya Naik, G. Nagaraju, Y. Shiralgi, *Sugarcane juice facilitated eco-friendly synthesis of solar light active $CdFe_2O_4$ nanoparticles and its photocatalytic application,* Eur. Phys. J. Plus (2018) 133: 229.

11.- K. Atacan, *$CuFe_2O_4$/reduced graphene oxide nanocomposite decorated with gold nanoparticles as a new electrochemical sensor material for L-cysteine detection*, J. Alloy. Compd. 791 (2019) 391-401.

12.- V. Narajan, A. Thayumanavan, *$CdFe_2O_4$ films for electroresistive detection of ethanol and formaldehyde vapors*, Microchim. Acta (2018) 185: 319.

13.- X. Li, P. Dong, C. Liu, X. Yu, J. Zhao, S. Sun, J. Liu, Y. Zhang, *The impact of the crystal structure and morphology on the electrochemical performance for $CuFe_2O_4$ in sodium ion batteries*, Ceramics Int. 44 (2018) 18471-18477.

14.- J. Wang, G. Yang, L. Wang, W. Yan, *Fabrication of one-dimensional $CdFe_2O_4$ yolk/shell flat nanotubes as a high-performance anode for lithium-ion batteries*, J. Mater. Sci.52 (2017) 4096-4108.

15.- R. Peymanfar, F. Azadi, *Preparation and identification of bare and capped CuFe2O4 nanoparticles using organic template and investigation of the size, magnetism, and polarization on their microwave characteristics,* Nano-Structures & Nano-Objects 17 (2019) 112-122.

16.-S. Ikram, J. Jacob, M.I. Arshad, K. Mahmood, A. Ali, N. Sabir, N. Amin, S. Hussain, *Tailoring the structural, magnetic and dielectric properties of Ni-Zn-CdFe2O4 spinel ferrites by the substitution of lanthanum ions,* Ceramics Int. 45 (2019) 3563-3569.

17.- B.D. Cullity and C.D. Graham, *Introduction to Magnetic Materials*, 2009 the Institute of Electrical and Electronics Engineers, Inc. DOI:10.1002/9780470386323 pp.180.

18.- D. S. Mathew, R.-S. Juang *An overview of the structure and magnetism of spinel ferritenanoparticles and their synthesis in microemulsions*, Chem. Eng. J. 129 (2007) 51–65.

19.- V. Vasanthi, A. Shanmugavani, C. Sanjeeviraja, R. Kalai Selvan, *Microwave assisted combustion synthesis of $CdFe_2O_4$: Magnetic and electrical properties*, J. Magn. Magn. Mat. 324 (2012) 2100-2107.

20.- H. Kaur, J. Singh, B.S. Randhawa, *Essence of superparamagnetism in cadmium ferrite induced by various organic fuel via novel solution combustion method*, Ceramics Int. 40 (2014) 12235-12243.

21.- M. Yokoyama, T. Sato, E. Ohta, T. Sato, *Magnetization of cadmium ferrite prepared by coprecipitation* J. Appl. Phys. 80 (1996) 1015.

22.- C.N. Chinnasamy, A. Narayanasamy, N. Ponpandian, R. Justin Joseyphus,K. Chattopadhyay, K. Shinoda, B. Jeyadevan, K. Tohji, K. Nakatsuka,H. Guérault, J.M. Greneche, *Structure and magnetic properties of nanocrystalline ferrimagnetic $CdFe_2O_4$ spinel*, Scr. Mater. 44 (2001) 1411–1415.

23.- M.H. Mahmoud, A.M. Abdallas, H.H. Hamdeh, W. M. Hikai, S.M. Taher, J.C. Ho, *Mössbauer spectroscopic evaluation of high-energy ball-milled $CdFe_2O_4$*, J. Magn. Magn. Mat 263 (2003) 269-274.

23.- R. Rai, K. Verma, S. Sharma, S.S. Nair, M. Almeida Valente, A.L. Kholkin, N.A. Sobolev, *Study of structural and ferromagnetic properties of pure and Cd doped cooper ferrite*, J. Phys. Chem. Solids 72 (2011) 862-868.

24.- G.F. Goya, H.R. Rechenberg, J.Z. Jiang, *Structural and magnetic properties of ball milled copper ferrite,* J. Appl. Phys. 84 (1998) 1101-1107.

25.- M. El-Hagary, A. Matar, E.R. Shaaban, M. Emama-Ismail, *The influence of Cd doping on the microstructure and optical properties of nanocrystalline copper ferrite film*, Mater. Res. Bull. 48 (2013) 2279-2285.

26.- R Rai, K. Verma, S. Sharma, S.S. Nair, M. Almeida Valente, A.L. Kholkin, N.A. Sobolev, *Structure and magnetic properties of Cd doped copper ferrite*, J. Alloy. Compd. 509 (2011) 7585-7590.

27.- P. P. Hankare, K. R. Sanadi, R. S. Pandav, N. M. Patil, K. M. Garadkar,. S. Mulla, *Structural, electrical and magnetic properties of cadmium substituted copper ferrite by sol–gel method* J. Alloy. Compd. 540 (2012) 290-296.

28.- G.V. Duong, R.Sato Turtelli, W.C. Nunes, E. Schafler, N. Hanh, R. Grössinger, M. Knobel, *Ultrafine $Co_{1-x}Zn_xFe_2O_4$ particles synthesized by hydrolysis: effect of thermal treatment and its relationship with magnetic properties*, J. Non-Cryst. Solids 353 (2007) 805-807.

29.- M. Veverka, Z. Jirak, O. Kaman, K. Knizek, M. Marysko, E. Pollert, K. Zavta, A. Lancok, M. Dlouha, S. Vratislav, *Distribution of cations in nanosize and bulk Co-Zn ferrites*, Nanotechnology 22 (2011) 345701.

30.- C. Gómez-Polo, V. Recarte, L. Cervera, J. J. Beato-López, J. López-García, J. A. Rodríguez-Velamazán, M. D. Ugarte, E. C. Mendonça, and J. G. S. Duque, *Tailoring the structural and magnetic properties of Co-Zn nanosized ferrites for hyperthermia applications*, J. Magn. Magn. Mat. 465 (2018) 211-219.

31.- R.Arulmurugan, G. Vaidyanathan, S. Sendhilnathan, B. Jeyadevan, *Thermomagnetic properties of $Co_{1-x}Zn_xFe_2O_4$ (x = 0.1-0.5) nanoparticles*, J. Magn. Magn. Mat. 303 (2006) 131-137.

32.- M. Veverka, P.Veverka, Z.Jirak , O.Kaman , K.Knızek, M.Marysko, E.Pollert, K.Zaveta, *Synthesis and magnetic properties of $Co_{1-x}Zn_xFe_2O_4$,nanoparticles as materials for magnetic fluid hyperthermia* J . Magn. Mag. Mat. *3*22 (2010) 2386–2389.

33.- P. Das, M. Colombo, D. Prosperi, *Recent advances in magnetic fluid hyperthermia for cancer therapy*, Colloid Surf. B-Biointerfaces 174 (2019) 42-55.

34.- Z.-Q. Zhang, S.-C. Song, *Thermosensitive/superparamagnetic iron oxide nanoparticle-loaded nanocapsule hydrogels for multiple cancer hyperthermia*, Biomaterials 106 (2016) 13-23.

35.-M. Moros, J. Idiago-López, L. Asín, E. Moreno-Antolín, L. Beola, V. Grazú, R. M. Fratila, L. Gutiérrez, J. Martínez de la Fuente, *Triggering antitumoral drug release and gene expression by magnetic hyperthermia*, Adv. Drug Deliv. Rev. 138 (2019) 326-343.

36.- P. Appa Rao, K. Srinivasa Rao, T.R.K. Pydi Raju, G. Kapusetti, M Choppadandi, M. C. Varma, K.H. Rao *A systematic study of cobalt-zinc ferrite nanoparticles for self-regulated magnetic hyperthermia*, J. Alloy. Compd. 794 (2019) 60-67.

37.- M. Munir Saiq, K. Suzuki, M.R. Hill, *Towards energy efficent separtions with meatl organic frameworks*, Chem. Commun. 54 (2018) 2825-2837.

38.-L. Menag, M. Munir Saiq, S.J.D. Konstas, K. Suzuki, , M.R. Hill, *Efficient delivery of oxygen via magnetic framework composites,* J. AMter. Chem. A 7 (2019) 3790-3796.

39.- C. Gómez-Polo, S. Larumbe, L.F. Barquín, L.R. Fernández, *Magnetic induction heating as a new tool for the synthesis of Fe_3O_4–TiO_2 nanoparticle systems*, J. Nanopart. Res. 18 (2016) 118.

40.- Y. Tao, G. Huang, H. Li, M.R. Hill, *Magnetic metal-organic framework composites:solvent-free synthesis and regeneration driven by localized magnetic induction heat*, ACS Sustain. Chem. Eng. 7 (2019) 13627-13632.

41.-C.C. Corten, M.W. Urban, *Repairing polymers using an oscillating magnetic field*, Adv. Mater. 21 (2009) 5011-5015.

42.- J. Huang, L. Cao, D. Yuan, Y. Chen, *Design of novel self-healing thermoplastic vulcanizates utilizing thermal/magnetic/light-triggered shape memory effects*, ACS Appl. Mater. Interfaces 10 (2018) 40996-41002.

43.- R. Panigrahi, M. Zarek, V. Sharma, d. Cohn, R.V. Ramanujan, Macromol. *Bio-inspired multiple cycle healing and damage sensing in elastomer-magnet nanocomposites*, Chem. Phys. 220 (2019) 1900168.

44.- Y. Yang, J. Ye, Q. Li, l. Gao, J. Hu, R. Zeng, J. Qin, S.X. Wang, Q. Wang, *Self-healing of electrical damage in polymers using superparamagnetic nanoparticles*, Nature Nanotech. 14 (2019) 151-155.

45.- J. Moriceau, P. Houzot, M. Pasturel, T. Gizouarn, T. Rouzel, *A magnetic glass matrix (ZnO-BaO-B_2O_3) particulate (Fe_3O_4) nanocomposite obtained by SPS*, J. Non-Cryst. Solids 514 (2019) 116-121.

46.- S. Hyder, V.M. Haq, *Thermomechanical characterization of nano-Fe3O4 reinforced thermoplastic adhesives and single lap-joints*, Compos. Pt. B-Eng. 175 (2019) 107162.

47.- S. Salimi, T.s. Babar, G.S. Dines, S.W. Baskerville, W. Hayes, B.W. Greenland, *Composite polyurethane adhesives that debond-on-demand by hysteresis heating in an oscillating magnetic field*, Eur. Polym. J. 121 (2019) 109264.

48.- P.M. Motersen, J.s. Engbaek, s.B. Vendelbo, M.F. Hansem M. Osberg, *Direct hysteresis heating catalytically active Ni-Co nanoparticles as stem reforming catalysts*, Ind. Eng. Chem. Res. 56 (2017) 14006-14013.

49.- J.M. Asensio, A.B. Miguel, P.F. Fazzini, P.W.N.M. van Leeuwen B. Chaudret, *Hydrodeoxygenation using magnetic induction: high-temperature heterogeneous catalysis in solution,* angew. Chem. Int. Ed. 58 (2019) 11306-11310.

50.-F.L. Rivera, F.J. Palomares, P. Herrasti, E. Mazario, *Improvement in heavy metal removal from wastewater using an external magnetic inductor,* Nanomaterials 9 (2019) 1508.

51.- J. Rodriguez-Carvajal, *Recent advances in magnetic structure determination by neutron powder diffraction*, Physica B 192 (1993) 55

52.- V.N. Nokoli, M. Valic, M.M. Milic, *Observation of low- and high-temperature $CuFe_2O_4$ phase at 1100℃: The influence of Fe^{3+} ions on the $CuFe_2O_4$ structural transformation*, Ceramics Int. 44 (2018) 21145-21152.

53.- M. Naseri, *Optical and magnetic properties of monophasic cadmium ferrite ($CdFe_2O_4$) nanostructure prepared by thermal treatment method*, J. Magn. Magn. Mat. 302 (2015) 107-113.

54.- A. Franco, H.V.S. Pessoni, F.L.A. Machado, *Spin-wave stiffness parameter in ferromagnetic systems: nanoparticle powders of (Mg, Zn)Fe_2O_4 mixed ferrites*, J. Appl. Hys. 118 (2015 173904.

55.-N. Modaresi, R. Afzlazadeh, B. Aslibeiki, P. Kameli, A. Gohotbi Varzaneh, I. Orue, V.A. Chernenko, *Magnetic properties of ZnxFe3-xO4 nanoparticles: A competition between the effects of size and Zn doping level*, J. Magn. Magn. Mat. 482 (2019) 206-218.

56.- C. Vázquez-Vázquez, M.A. López-Quintela, M.C. Buján-Núñez, J. Rivas, *Finite size and surface effects on the magnetic properties of cobalt ferrite nanoparticles*, J. Nanopart. Res. 13 (2011) 1663-1676.

57.- H. Parmar, P. Acharya, R.V.Upadhyay, V.Siruguri, S. Rayaprol, *Low temperature magnetic ground state in bulk $Co_{0.3}Zn_{0.7}Fe_2O_4$ spinel ferrite system: Neutron diffraction, magnetization and ac-susceptibility studies,* Solid State Commun.153 (2013) 60-65.

58- G.F. Goya, T.S. Berquó, F.C.,Fonseca, M.P. Morales *Static and dynamic magnetic properties of spherical magnetite nanoparticles.* J. Appl. Phys. 94 (2003) 3520–3528.

59.- 37.- S. Chikazumi, *Physics of Magnetism*, Wiley 1964, p. 277.

60.- J. Kurian, M. Jacob Mathew, *Structural, optical and magnetic studies of $CuFe_2O_4$, $MgFe_2O_4$ and $ZnFe_2O_4$ nanoparticles prepared by hydrothermal/solvothermal method. J. Magn. Magn. Mat.* 451 (2018) 121-130.

61.- I. Andreu, E. Natividad, *Accuracy of available methods for quantifying the heat power generation of nanoparticles for magnetic hyperthermia*, Int. J. Hyperthermia 29 (2013) 739-751.

62.-C.N.Chinnasamy, A. Narayanasamy, N. Ponpandian, R. Justin Joseyphus, B. Jeyadevan, K. Tohji, K. Chattopadhyay, *Grain size effect on the Néel temperature and magnetic properties of nanocrystalline $NiFe_2O_4$ spinel*, J. Magn. Magn. Mat. 238 (2002) 281-287.

63.- D. Ravinder, *Electrical transport properties of cadmium substituted copper ferrites*, Mater. Lett. 43 (2000) 129-138.